Ozone Interaction with Polycyclic Aromatic Hydrocarbons and Soot in Atmospheric Processes: Theoretical Density Functional Study by Molecular and Periodic Methodologies

Andrea Maranzana,[†] Giovanni Serra,[†] Anna Giordana,[†] Glauco Tonachini,*[,†] Gianluca Barco,[†,‡] and Mauro Causà*[,‡]

Dipartimento di Chimica Generale ed Organica Applicata, Università di Torino, Corso Massimo D'Azeglio 48, 10125 Torino, Italy, and Dipartimento di Scienze dell'Ambiente e della Vita DISAV, Università del Piemonte Orientale "Amedeo Avogadro", Piazza Ambrosoli 5, 15100 Alessandria, Italy

Received: July 5, 2005; In Final Form: September 26, 2005

The ozonization mechanism for polycyclic aromatic hydrocarbons (PAHs) and soot is investigated by quantum mechanical calculations carried out on molecular and periodic systems. PAHs, interesting per se, serve also to model the local features of the graphenic soot platelets, for which another model is provided by a periodic representation of one graphenic layer. A concerted addition leads to a primary ozonide, while a nonconcerted attack produces a trioxyl diradical (in which one of the two unpaired electrons is π-delocalized). Easy loss of (i) $^1O_2$ or (ii) $^3O_2$ from either intermediate, with spin conservation, would yield stable (i) singlet or (ii) triplet π-delocalized species which carry an epoxide group. The trioxyl diradical pathway is estimated to be preferred, in these systems. An intersystem crossing, taking place in the trioxyl diradicals, can be invoked to allow the even easier loss of a ground-state oxygen molecule with the formation of a ground-state epoxide in a more exoergic and less demanding step. We propose that soot ozonization can take place by such a process, with ultimate functionalization of the graphenic platelets by epoxide groups.

1. Introduction

Large quantities, ca. 13 Tg, of black carbon (soot, elemental carbon) are emitted into the troposphere during the year as a consequence of the combustion of biomass and fossil fuel.[1a] Soot aerosol contributes in a significant way to the total mass of atmospheric aerosol. It has an irregular agglomerate structure of graphene layers, and both its structure and composition can vary depending on the source.[1b,2] These irregular sheets are clustered in globular particles, whose dimensions vary between 10 and 80 nm, approximately. In any case, a relatively large area of the particles is available to the interactions with airborne inorganic and organic molecules. In recent times, the interaction of soot with small inorganic oxidants, as NO_2,[3−5] HNO_3,[3] H_2O,[6] and O_3,[6−8] as well as the oxidation of polycyclic aromatic hydrocarbons (PAHs)[5] on soot, have been investigated experimentally. PAHs and their derivatives (PACs, polycyclic aromatic compounds) are ubiquitous species, whose presence is widespread: beyond being produced from a variety of combustion sources, they are known as primary and secondary tropospheric pollutants, especially in urban areas.[1] This means that oxidation can take place either already during combustion or at a later time, during the tropospheric transport of a combustion-generated particulate. As PAHs and PACs are generated in the same combustion processes at low O_2 concentrations that bring about the more or less disordered growing of the graphenic layers, they share the same nature of soot.[1,2] Since PACs have been detected in diesel exhaust, they have even also been hypothesized to possibly originate on the surface of particulate matter. Because of the origin and structural affinities, they are often times found,[1c] and their chemistry studied, in association with carbonaceous particulates.[6,9] The functionalization of PAHs and that of soot could share some mechanistic features.

The functionalization of PAHs, and soot itself, has been studied both by field campaigns and by laboratory studies.[10] It has been observed that, while transported, different PAHs decay at very different rates. As a consequence, the relative amount of carcinogenic/mutagenic primary products changes significantly and other products form. Their nature is in some cases known, in others it is not.[11] Therefore, the transformation of primary pollutants, either through gas phase reactions or by heterogeneous processes (via their interaction with the fine particulate), is of great interest from the chemical and toxicologic points of view. One important aspect is that as the compound or particle polarity increases, so does its water solubility and it can be more easily brought into contact by the aerosol with, for instance, the lung tissues. Therefore, PAHs and PACs adsorbed on fine particles are of concern regarding human health.[1d]

The interaction of O_3 with soot could be important for both tropospheric and stratospheric chemistries. On one hand, tropospheric ozone is one of the possible candidates for starting the oxidation of primary soot, which plays an important role in the atmospheric chemistry of secondary aerosol and in nucleation phenomena.[12a] On the other hand, aerosol passing in due course through the tropopause, or produced directly in the stratosphere, might give way to reactions with stratospheric ozone. This point is discussed by Kamm, Mohler, Naumann, Saathoff, and Schurath (KMNSS) in a 1999 study on soot−ozone interaction.[8] The authors actually point out that "very low black carbon concentration of the order of $\approx$1 ng/m^3 had been observed in the upper troposphere and lower stratosphere".[12b] Then, they conclude that ozone depletion on dry soot aerosol

* To whom correspondence should be addressed. E-mail: glauco.tonachini@unito.it. Fax: ++39−011−6707642. Website: http://www.thecream.unito.it/. E-mail: causa@al.unipmn.it. Fax: ++39-0131-287416. Website: http://www.mfn.unipmn.it/∼causa.

† Università di Torino.

‡ Università del Piemonte Orientale.

10.1021/jp053672q CCC: $30.25
Published on Web 11/09/2005

is negligible both in the troposphere and in the lower stratosphere. KMNSS investigated the interaction of ozone with Palas soot. They modeled the observed concentration and time dependencies of the ozone loss rate by four quasi-elementary reactions: (1) rapid destruction of one monolayer equivalent of ozone on pristine surface sites, (2) ozone-induced and (3) spontaneous recovery of reactive sites, and (4) spontaneous site passivation. It must also be mentioned that Fendel, Matter, Burtscher, and Schmidt-Ott (FMBSO) had previously studied, in 1995, the kinetics of the initial fast step of the soot−ozone interaction.[7]

It is to reaction 1 of KMNSS that our theoretical investigation bears relevance. Thus, the interaction of O_3 with some model systems is studied here also with the aim of offering an interpretation to the laboratory results of KMNSS, which are relevant to atmospheric chemistry. To this end, this first study on PAH and soot ozonization takes into account O_3 attacks on the internal region of the model systems. Work is in progress on the complementary border reactivity, and this aspect will be discussed in a forthcoming paper. Investigating the nature of the interaction of ozone with the surface of soot particles by theoretical means, studying in particular the mechanistic details of ozonization, could be instrumental for a better understanding of some tropospheric processes and can be seen as complementary to the valuable data collected experimentally. The present study is preceded by a first paper[13] in which we attempted to define a suitable model for soot and examined the features of the interaction of some small species (H, NO, NO_2, and NO_3) and the gas−solid interaction by which functionalization reactions can take place. Here, quantum mechanical calculations are first carried out on molecular PAH-type systems. The reactions studied are actually gas-phase reactions, such as those already examined in this laboratory,[14] which can be interesting by themselves but are expected in this case to be helpful in setting up a model for the reactivity of a soot platelet. The computations are then further extended to a periodic representation of an undefective (functionalized) graphene layer, which stretches to infinity in two directions. Although it can be seen as an extreme on the size scale, it is also instrumental (by flanking the small molecular systems) to attempt to model a platelet belonging to a soot particle. In this respect, some recent work along the same line can be mentioned.[15−17]

2. Methods

The stable and transition structures (TS) were determined by gradient procedures[18a] within the density functional theory (DFT) and making use of the B3LYP functional.[19] This functional is of widespread use and, even if prone to underestimate some reaction barriers, has generally performed well regarding geometries and energetics.[20] The polarized 6-31G(d)[21] and 6-21G(d)[22] basis sets were used in the DFT (B3LYP) optimizations. The 6-21G(d) basis set was applied in periodic models because it gives a larger variational freedom in optimizing the external s−p Gaussians in the periodic calculation. The nature of the critical points was checked by vibrational analysis; this was carried out only for the most important critical points in the case of the largest system (M42, see below). In the case of transition structures, inspection of the normal mode related to the imaginary frequency was sufficient to confidently establish its connection with the initial and final energy minima. For one transition structure (^{1}TCD−EPO, see below), an IRC calculation[18b] helped to confirm the connection with the adjacent energy minimum. For the preferred pathway (see below), the energy evaluations were refined by using a more extended basis set, the 6-311G(2d).[21]

Some of the intermediates encountered in this study have diradical character. As already noted in previous studies,[1] unrestricted DFT (UDFT) calculations on singlet diradicals converge on incorrect closed-shell-type solutions, with zero spin densities and $\langle \hat{S}^2 \rangle = 0$ (ψ_0). To get a qualitatively correct picture of a singlet diradical in terms of nonzero spin densities, the UDFT monodeterminantal wave function had to be handled in the following way: (1) A wave function stability test was carried out on ψ_0. Since it came out to be unstable with respect to orbital rotations, it was allowed to relax along the instability direction and a new stable solution was found.[2] (2) The resulting wave function has nonzero spin densities, as expected for a singlet diradical and $\langle \hat{S}^2 \rangle \approx 1$ (ψ_1): this results indicates that relaxation allows the triplet ($\langle \hat{S}^2 \rangle = 2$) to mix in. (3) In correspondence with the stable wave function, the critical points (minima, saddle points) are identified on the E_1 hypersurface so obtained. (4) Because of this spin contamination, one may want to refine the E_1 values which correspond to the critical points. To this purpose, the formula suggested by Yamaguchi[3] allows one to get rid of the closer spin contaminant (i.e., the triplet, if a singlet is concerned) and obtain the "final" E, which is an approximate estimate. Since this is a composite treatment (and no definition of a critical point can be made in correspondence of E, the refined-energy hypersurface), in the presence of small ΔE_1 differences, it is possible that an unpleasing reversal of the sign takes place when ΔE is obtained. However, we deem this reversal not very important from a chemical point of view, as will be discussed in the next section. Finally, the energies were combined with the thermochemical corrections from the vibrational analysis (using unscaled vibrational frequencies)[4] to get estimates of the activation and reaction enthalpies and free energies (complete only for the two smaller systems, M16 and M24 (see below)). The relevant energy and free energy differences are collected in Table 1. A more complete set of energies, enthalpies, entropies, and free energies are presented, together with the relevant critical point geometries and some spin densities, in the Supporting Information.

All molecular calculations were carried out by using the GAUSSIAN 2003 system of programs.[27]

The periodic LCAO calculations were performed by using the CRYSTAL 2003 program:[28] structures periodic in three (bulk crystals), two (slabs), and one dimension (polymers) can be treated by using Hartree−Fock, density functional, and hybrid Hamiltonians. The periodicity is fully considered by using cyclic-boundary conditions: the infinite series of Coulombic integrals are approximated by Ewald techniques[29] while the infinite exchange series, representing an essentially short-range interaction, are truncated while ensuring convergence on the energy and related observables.[30] The solution of the effective one-electron Schroedinger equations is performed in the reciprocal space. The K-points are sampled on a regular mesh: for conducting systems, the Fermi surface is calculated using a denser K-point mesh, using Fourier interpolation of energy bands.[31] The symmetry is fully implemented in the direct space, to minimize the number of molecular integrals to compute and to store, and in the reciprocal space, to perform a block diagonalization.[32] Recently, energy derivatives with respect to the position of the atoms in the unit cell have been implemented in CRYSTAL, and an automatic optimization of the equilibrium geometry, within a given crystal symmetry, is possible.[33]

3. Results and Discussion

The lack of structural information on the atomic scale about soot and its possibly active surface sites (useful to set up a

TABLE 1: Energies[a] and Free Energies[a] of the Initial Transition Structures and Intermediates

substrate[b] / structure[c]		M16	M24	M42
R−PO		26.7 (39.0)	26.2 (38.8)	18.4 (30.9)
PO		16.4 (30.3)	16.4 (30.8)	5.1 (19.8)
PO− EPO		37.2 (47.9)	37.6 (48.7)	27.2 (37.6)
R−^{1}TCD	E_1	19.4 (29.7)	18.1 (28.8)	12.7 (23.3)
	E	*17.5 (27.8)*	*16.3 (27.0)*	*10.3 (20.9)*
^{1}TCD syn	E_1	19.3 (29.5)	17.2 (27.8)	11.7
	E	*18.6 (28.7)*	*16.6 (27.2)*	*11.2*
^{1}TCD anti	E_1	18.6 (28.4)	17.2 (27.4)	11.6 (21.8)
	E	*19.1 (28.9)*	*17.6 (27.7)*	*11.8 (22.1)*
^{1}TCD−^{3}OCD[d,e]	E_1	19.2 (28.4)	17.8 (27.5)	12.2
	E	*20.3 (29.5)*	*18.7 (28.3)*	*(12.7)*
^{3}OCD[e]		14.1 (12.1)	13.8	8.6
^{1}TCD−EPO[d]		22.3 (31.0)	21.2 (30.3)	13.8
			18.9 (28.0)	
^{3}TCD		18.1 (27.3)	16.8 (26.5)	11.4
^{3}TCD−EPO[d]		18.2 (26.9)	16.9 (26.1)	11.7
EPO[e,f]		[−17.7][g]	−15.0 (−14.5)	−23.9
oxepine[e,f]		−29.3[g] (−28.2)	−20.9 (−19.8)	

[a] Relative to the reactants; free energies are in parentheses. Singlet diradicaloid structures: each first line reports the unrefined energy E_1, while values in italic (second line, *E*) are the result of the Yamaguchi energy refinement (ref 25), as outlined in the Methods section; all values in kcal mol^{-1}. [b] See Figure 1. [c] Labels, see Scheme 1. Transition structures are identified by the labels of the minima they connect. [d] From anti-TCD. [e] Plus $^3O_2$. [f] The products (EPO + $^1O_2$) or (oxepine + $^1O_2$) would have the energy difference between $^1O_2$ and $^3O_2$ (20.9 kcal mol^{-1}, at this computational level) added to each entry. [g] The epoxide ring spontaneously opens upon cleavage of the C−C bond and gives an oxepinic ring; by holding the C−C bond frozen to 1.58 Å, this is prevented and the bracketed value is obtained.

computational study and for subsequent comparative purposes) poses some difficulties in setting up adequate models. Only a few experimental studies report on this issue to some extent.[8,12] Both the molecular and the periodic models considered in this paper are in principle dimensionally inadequate, for opposite reasons: soot is made up of finite graphene layers larger than our PAH molecular models, yet not stretching out infinitely in two dimensions, as our periodic models do. Nevertheless, if these two models will provide consistent information about the local chemical behavior (as was the case in our previous paper),[13] they will be deemed helpful in describing local chemical features of soot particles.

Some aromatic hydrocarbons have been chosen as molecular models and compared. All PAH models have an even number of carbon and hydrogen atoms and share the same spin multiplicity (singlet) with the periodic models. They have been labeled M*n* for short, where *n* is the number of carbon atoms. First comes pyrene, $C_{16}H_{10}$, labeled M16, followed by coronene, $C_{24}H_{12}$, M24, and by tetrabenzo[hi,jk,st,uv]ovalene, $C_{42}H_{16}$, M42 (Figure 1). The simplest PAH, naphthalene (M10), is mentioned here on occasion, just for comparative purposes (though the carbons shared between the two rings are tertiary, they do not correspond to completely internal positions).

The periodic models are set up by defining two-dimensional (2D) supercells. The substrate is represented by a number of atomic layers. The convergence of the surface properties vs the number of atomic layers is normally fast, due to the exponential decay of the surface electrostatic field orthogonally to the surface. The neighboring layer influences only weakly the electronic structure, as can be shown by theoretical and experimental studies of graphite scanning tunneling microscope images.[15] On the other hand, a single graphene layer can describe the surface chemical properties of graphite.[34,35] Therefore, each periodic model is one single layer of hexagonal graphite with cyclic boundary conditions in two dimensions. Supercells P$\sqrt{3}\times\sqrt{3}$ and P3×3 have been analyzed, as reported in the Figure 2.

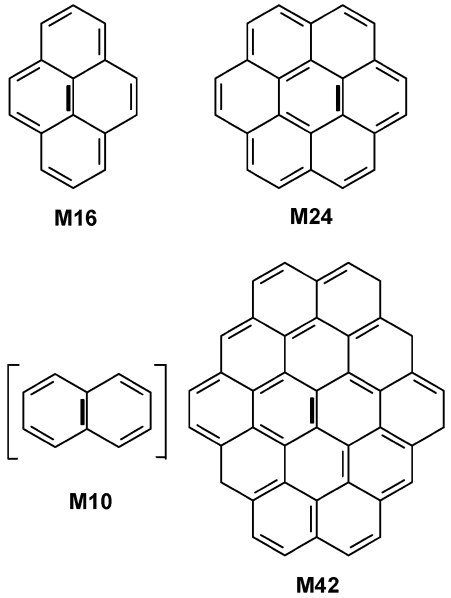

Figure 1. Molecular models adopted in the study: pyrene (M16), coronene (M24), and tetrabenzo[hi,jk,st,uv]ovalene (M42). The π-bonds attacked by ozone in our models are in bold.

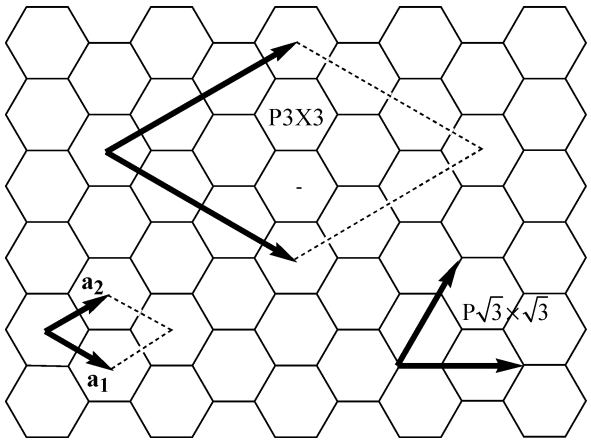

Figure 2. Periodic models: 2D unit cell and supercells ($\mathbf{a}_1$ and $\mathbf{a}_2$ are the fundamental lattice vectors), P$\sqrt{3}\times\sqrt{3}$.

In the following, the possible reaction pathways will be considered (Scheme 1). The intermediate and transition structures species have been labeled for convenience by bold acronyms, as detailed in the legend. Actually, the results of our hypersurface study simplify to some extent the rather complex scheme: in fact, the parts included in dashed boxes correspond to structures which can be conceived but have not been found as energy minima or transition structures.

The π-bonds directly involved in the gas-phase addition of ozone to the unsaturated systems are marked in bold in Figure 1, where the M*n* models are displayed (obviously, six equivalent positions are present in M24). The addition could take place in either a synchronous or asynchronous concerted way or by a two-step process (Scheme 1). While any concerted attack leads directly to the primary ozonide (PO) intermediate (with a local 1,2,3-trioxolane structure, § 3.1), the latter produces an open-chain trioxyl cyclohexadienyl-like diradical, TCD (§ 3.2).

SCHEME 1: Formation of Either the Primary Ozonide (PO) of the Unsaturated System or Its Trioxyl Cyclohexadienyl-like Diradical (TCD) and Subsequent Bond Breakings, Ring Closures, and O_2 Loss

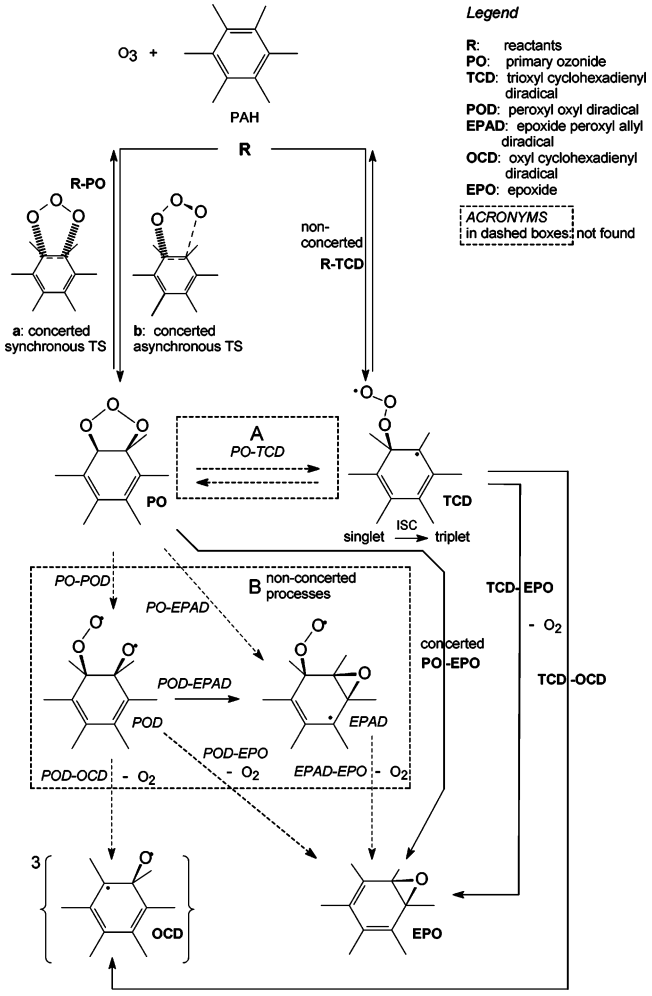

3.1. Formation of the Primary Ozonides. The M*n* models allow the ozone attack on a couple of atoms shared by four benzo groups: this means that no border atoms are involved (naphthalene is of course an exception). All R−PO transition structures are found to correspond to rather synchronous concerted additions, as witnessed by the rather similar C−O distances, which differ in the same transition structure at most by 0.005 Å and are 1.86 Å for M16 and M24 and 1.87 Å for M42. The primary ozonides are well-defined minima on the potential energy surface. The energy barriers for PO formation and the PO stability with respect to the reactants R are reported in Table 1. The PAH models indicate an endoergic behavior, due to the partial loss of aromatic character. The step seems to become less endoergic as the system gets from M16 and M24 to the more extended M42. For M16 and M24, PO formation requires overcoming a substantial barrier, somewhat larger than 26 kcal mol^{-1} and the energy minima are ca. 16 kcal mol^{-1} above the reactants. The larger M42 presents a barrier of 18 kcal mol^{-1}, and its PO is located only 5 kcal mol^{-1} above the reactants. Part of the energy cost can be attributed to the pyramidalization and change in hybridation of the attacked carbons. As the system extends, part of the strain can be partitioned over a larger series of bonds and angles. With regards to the stability of PO, the periodic models (Table 2) span the range from 8 to −4 kcal mol^{-1}. The molecular and periodic models appear to provide a similar qualitative physical description.

TABLE 2: Periodic Calculations: Energies[a] of the Intermediates

structure[b]	PO	^{3}TCD	EPO
P$\sqrt{3}\times\sqrt{3}$	8.0	8.0	−22.7
P3×3	−4.0	3.1	−23.4

[a] kcal mol^{-1}. [b] See Figure 2.

On the other hand, it can be seen that the attacks on positions close to the border (naphthalene) are definitely different. For M10, the barrier is 22.3 kcal mol^{-1} and PO is located 6.5 kcal mol^{-1} higher than the reactants. For the attack on border positions (paper in preparation), the step can even be exoergic. This could be attributed at least in part to the easier carbon pyramidalization but could also be due to a higher electron density, to which ozone (an electrophile) is sensitive.

The difference in formation energy for the primary ozonides in the periodic models reveals that the PO on a graphite sheet could have some thermodynamical stability only at very low coverages. P3×3 corresponds to one ozone molecule for every 9 unit cells, that is each 18 carbon atoms. At a higher coverage, the electrostatic repulsion between the ozone molecules renders the absorbed phase too unstable. An analysis of the adsorption energy shows that the short-range repulsion between chemisorbed molecules is neglibible (below 0.6 kcal mol^{-1} for the P$\sqrt{3}\times\sqrt{3}$ phase, below 0.01 for the P3×3 phase). On the other hand, the electrostatic repulsion between the adsorbed O_3 molecules is 4.0 kcal mol^{-1} in the P3×3 phase but becomes 16.0 kcal mol^{-1} in the P$\sqrt{3}\times\sqrt{3}$ phase, so explaining the larger part of the difference between the PO formation energy of the periodic models.

3.2. Formation of the Trioxyl Diradical. The ozone attack to the PAH can also be nonconcerted. In this case, only one C−O bond forms and a singlet trioxyl diradical (^{1}TCD) results with spin conservation, in which one unpaired electron is largely on the terminal oxygen, with a smaller contribution from the adjacent oxygen, while the second unpaired electron is delocalized in the π-system (as can be evinced by inspecting the spin densities, see the Supporting Information). Since in the case of benzene it would be a trioxyl cyclohexadienyl diradical, the acronym TCD is used here also for its larger analogues (cyclohexadienyl-like diradicals). Its wave function and energy are defined as described in the Methods section. The difference between their E_1 values and the final E values obtained through Yamaguchi's formula[25] is not very different (0.4−0.7 kcal mol^{-1}). Each diradical is somewhat less stable than the corresponding PO: ^{1}TCD is located ca. 17−19 kcal mol^{-1} above the reactants for M16 and M24, vs ca. 16 kcal mol^{-1} for PO. For M42, both values are appreciably lower, 11−12 kcal mol^{-1} (^{1}TCD), to be compared with 5 (PO). However, the diradical formation transition structures (R−TCD in Scheme 1 and Table 1) lie at energies significantly lower than those of the corresponding R−PO transition structures, by 7−5 kcal mol^{-1}. Yet, the barriers for the reverse process, back to R, are quite small for the TCD intermediates, or even nonexistent, if, instead of E_1, the E value obtained by the Yamaguchi energy refinement[25] is taken (Table 1). These data suggest (by taking into account the limitations of the computational method outlined in the Methods section) that the role of the diradicals as real intermediates on the reaction pathway is very questionable, but does not rule out the possible importance of a "diradicaloid pathway", as will be discussed in the next subsections.

SCHEME 2

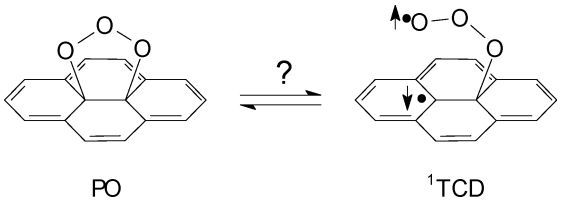

3.3. Primary Ozonide-Trioxyl Diradical Interconversion. The PO adduct can be thought of as a vibrationally excited species, PO*. The addition step entails some excess energy that can result either in a backward step or in the cleavage of a single bond, depending on the distribution of the energy among the vibrational modes. If the C−O symmetric stretching ($r_1 + r_2$) is obviously related to the formation/decomposition of PO, then its antisymmetric counterpart ($r_1 - r_2$) would possibly connect PO with its singlet trioxyl diradical isomer ^{1}TCD, via a possible transition structure PO−TCD. Therefore, to complete the picture of these initial steps, we have investigated the possible PO ⇄ TCD interconversion (Scheme 2).

A thorough search for an interconversion TS gave the result that this process cannot take place directly. Both PO and ^{1}TCD can interconvert only by dissociating back to the reactants R. The search involved several steps that can be examined with the help of Figure 3, in which the data for pyrene are displayed (similar results were obtained for coronene). First, a direct TS search was attempted and failed to locate a critical point. However, a direction along which the energy surface presents a negative curvature was identified, approximately coincident with r_1, the C−O bond to be cleaved when going from PO to ^{1}TCD. Then, several constrained searches for a first-order saddle point, carried out at different fixed values of the r_2 parameters (ranging from 1.35 to 1.90 Å) allowed us to locate a ridge, initially positioned in correspondence with an almost constant value of $r_1 \approx 2.07$ Å, then decreasing down to ca. 1.8 Å (Figure 3a, black diamonds). Along this ridge, all forces were below the fixed threshold, with the exception of that along the r_2 coordinate. Now, if a real TS were present, then the ridge itself should present a minimum along r_2. This was not found: though the section of the energy surface along the ridge (Figure 3b) has positive curvature, it is all the way downhill, with a decreasing value of the force along the r_2 coordinate. When the value of r_2 is increased beyond 1.7 Å, the ridge bends and leads smoothly toward the R−PO transition structure. In other words, if one C−O bond in PO stretches, this, instead of leading toward the ^{1}TCD minimum, triggers the cleavage of the other C−O bond as well. This behavior could be reminiscent of the β-fragmentation process in radicals, since, upon C−O bond stretching, its two electrons decouple and an incipient unpaired electron is found adjacent to the other C−O σ-bond and weakens it.

The consequence of this trait of the energy hypersurface is that the attack leading to ^{1}TCD seems at first sight favored. Yet, ^{1}TCD itself seems more inclined to back dissociate to the reactants. However, the data were at that point still incomplete. Once the complete pathways were defined, a steady-state treatment was carried out, to assess their competition (see below).

Other evolutions of PO can be envisaged (Scheme 1), all of them within the singlet spin multiplicity. The cleavage of one O−O bond would possibly produce a peroxyl oxyl diradical POD (through the transition structure PO−POD). If the same O−O bond cleavage were accompanied by a three-ring closure, the epoxide peroxyl allyl diradical EPAD would form (via the transition structure PO−EPAD). EPAD could also form in two steps, via POD. Finally, both POD and EPAD could give way to an epoxide EPO by the loss of an oxygen molecule. Actually, the investigation of the energy surface simplified drastically this rather intricate picture. The POD intermediate could not be found for the internal positions of the M*n* models, because an O_2 moiety tends to spontaneously dissociate. Given that the present work is focused on the reaction mechanisms for the ozone oxidation of PAHs or soot platelets in internal positions (i.e., oxidation of tertiary aromatic carbons), the POD structure appears to be irrelevant to this case. With regards to the EPAD intermediate, similar results have been collected. For naphthalene, it is less stable than the reactants by 9.7 kcal mol^{-1} (and the relevant TS PO−EPAD is 18.5 kcal mol^{-1} above PO). Again, no such structures could be located as energy minima on the hypersurfaces of the M*n* models, since dioxygen spontaneously dissociates again, leaving an EPO structure. With regards to the oxyl cyclohexadienyl-like diradical, OCD, no such structure exists on an internal position within the singlet multiplitiy. In fact, it spontaneously gives ring closure to EPO. However, one could imagine the formation of ^{3}OCD from ^{1}TCD,

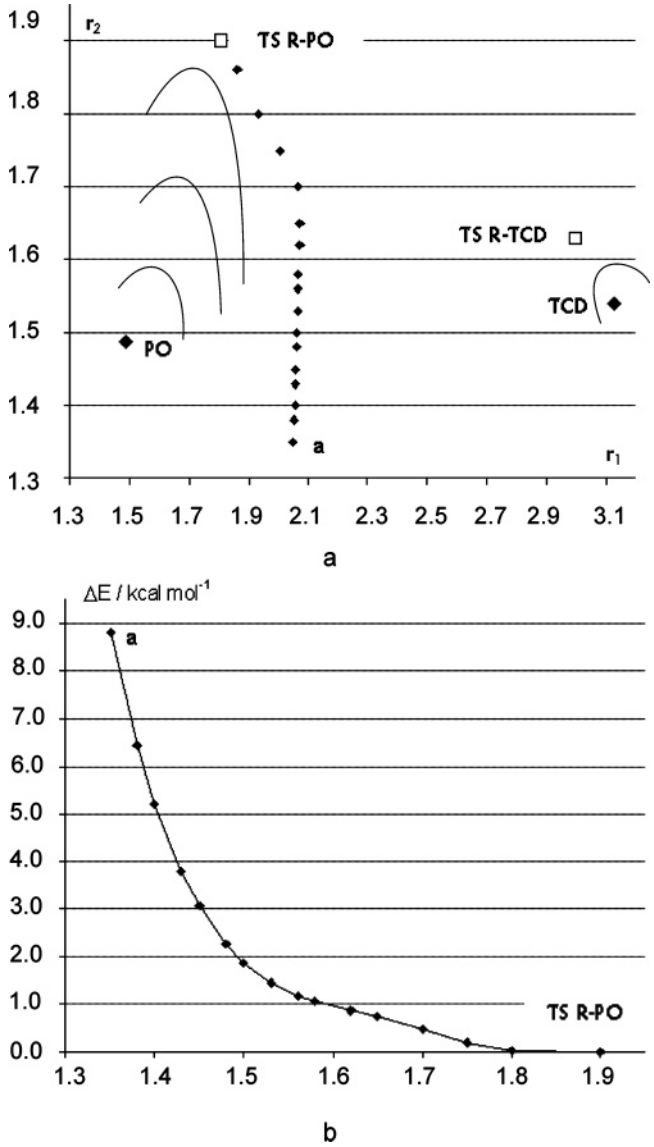

Figure 3. (a) Map of the ridge (**a**, black diamonds) zone, which separates the dominium of PO from that of ^{1}TCD (minima as black diamonds, transition structures as white squares) and (b) energy, relative to the R−PO transition structure, along ridge **a**.

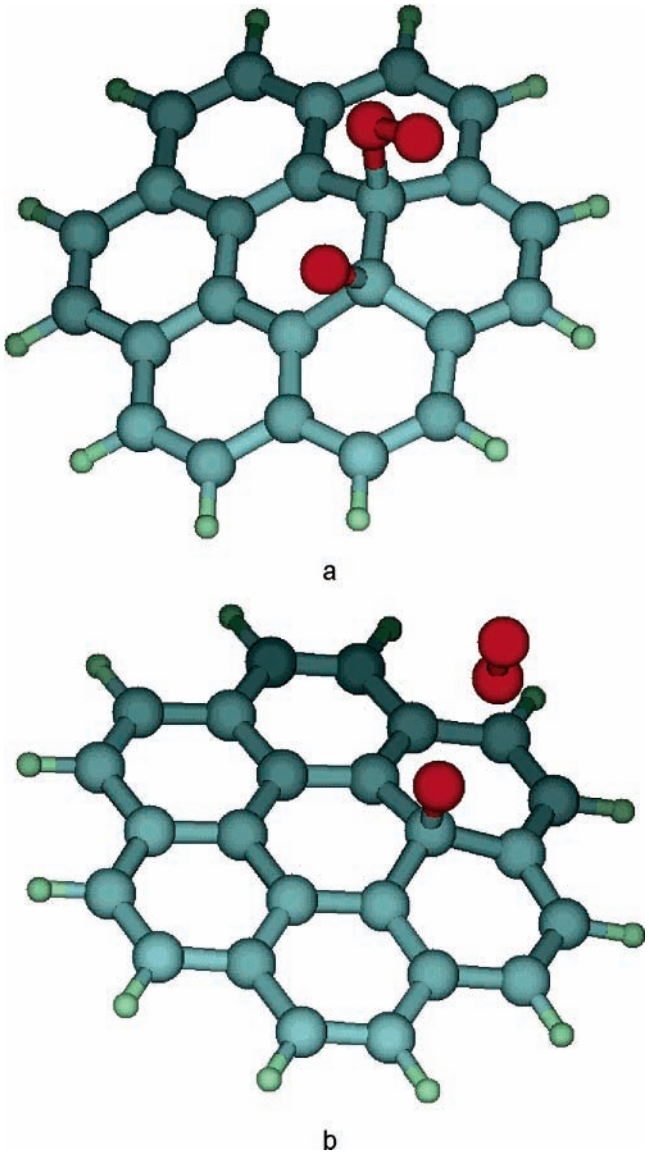

Figure 4. Two transition structures for M24: (a) PO−EPO, connecting the primary ozonide to the final epoxide via O−O bond cleavage (and subsequent C−O bond cleavage with the loss of singlet dioxygen) and (b) ^{1}TCD−^{1}EPO connecting the trioxyl diradical to the final epoxide via O−O bond cleavage and the loss of singlet dioxygen.

as a consequence of the detachment of triplet dioxygen. Table 1 shows that the barrier for the transformation ^{1}TCD−^{3}OCD (+ $^3O_2$) would be low. Once formed, ^{3}OCD could close to EPO only if an intersystem crossing occurs.

3.4. From the Primary Ozonides to the Epoxides. These results leave the fully concerted "dioxygen loss and closure of one epoxide ring" step as the only possible functionalization pathway originating from PO. However, the related barrier is significant in all cases, since the PO−EPO transition structure is higher than PO by 20.8 kcal mol^{-1} in terms of *E* and 17.6 in terms of *G* (M16), by 21.2 and 17.9 (M24), and by 22.1 (*E*, M42). The transition structure ^{1}PO−^{1}EPO is shown in Figure 4a for M24.

With regards to the geometric features of this transition structure, one can notice that the three main changes which take place in a concerted manner do not appear to be synchronous. The breaking O−O bond is significantly stretched: 2.445 Å (M16), 2.558 Å (M24), and even 2.981 Å (M42). By contrast, the C−O bond, which is also cleaved, is only 1.575 Å long (M16), 1.583 Å (M24), and 1.668 Å (M42). Similarly, that OCC angle, which is closing to give the epoxide ring, is still 80.8° wide (M24) and 80.0° (M42), which can be compared to the final values in the epoxides, 56.5° and 58.6°, repectively. For M16 (initial ∠OCC value, 82.7°), the situation is somewhat different, because the epoxidic structure is unstable and the C−C bond cleaves, giving an oxepinic ring (final ∠OCC value, 39.9°).

SCHEME 3: Outline of the Possible Flanking of the Original Singlet Pathway by a Triplet Pathway Generated by an Intersystem Crossing

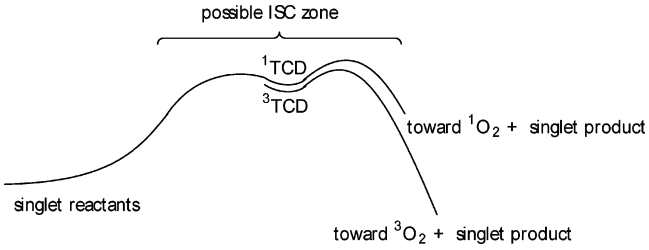

3.5. Diradicaloid Pathways to the Epoxide (oxepine). An alternative pathway can go through the ^{1}TCD diradical, or given that its existence as a real intermediate appears dubious, we could more loosely say "through a corresponding diradical region" and avoid making explicit reference to an intermediate. However, for the sake of simplicity, reference will be plainly made in the following to ^{1}TCD, with that caveat in mind. From ozone and the PAH (both singlets), ^{1}TCD can form with conservation of the total spin. From ^{1}TCD, dioxygen loss takes place rather easily (with ΔE_1 barriers of 3.7 kcal mol^{-1} for M16, vs 4.0 for M24, and 2.2 for M42 with respect to the energy minimum). These values correspond to overall barriers of 22, 21, and 14 kcal mol^{-1}, respectively. The use of the refined ΔE values for the barriers is limited to coronene, since the other two systems present significantly contaminated triplets for TS ^{1}TCD−^{1}EPO, which do not allow the use of the procedure.

If spin is conserved, O_2 must form from ^{1}TCD in a singlet state (TS ^{1}TCD−^{1}EPO), unless the triplet multiplicity is induced in the π-system of the product epoxide by the formation of ground-state O_2 (the two triplets coupled to give an overall singlet, TS ^{1}TCD−^{3}EPO). However, the energies involved are substantial (more than 30 kcal mol^{-1} as difference between ^{1}EPO and ^{3}EPO). Otherwise, triplet dioxygen and a triplet oxyl cyclohexadienyl diradical (^{3}OCD) could form, coupled again to an overall singlet (Table 1). Still another evolution of the system is possible, if ^{1}TCD undergoes an ISC prior to the O−O bond cleavage (giving ^{3}TCD) or in the course of it (Scheme 3).

As a consequence of ISC, ^{3}TCD could give way to both ground-state triplet oxygen and an ^{1}EPO molecule (TS ^{3}TCD−^{1}EPO). Given the comparable energy of the singlet and triplet TCD diradicals, the close similarity of their geometries, and the closeness of their vibrational frequencies, ISC appears to be a realistic possibility. The quantitative study of this aspect is currently under way and will be published separately.[36] ^{3}TCD could also give singlet dioxygen and ^{3}OCD, but this is by far less energetically advantageous than producing $^3O_2$ and the ground-state epoxide.

The actual product is an ether in all cases. However, if the EPO structure is stable for M24 and M42, then only an oxepine can be found for the smaller M16 because the carbon−carbon bond potentially involved in the epoxidic cycle spontaneously cleaves. Just to assess the energy of an epoxidic structure, a constrained optimization was also carried out for M16 (see Table 1).

With regards to the main geometric features of the mentioned transition structures, that is, the oxygen−oxygen distance for

TABLE 3: Main Geometrical Parameters[a] for the O_2 Loss Transition Structures from TCD

substrate	M16	M24	M42
^{1}TCD−^{1}EPO[b]			
O−O	1.875	1.889	1.820
∠OCC	89.7	90.1	91.1
^{1}TCD−^{3}OCD[b]			
O−O	1.758	1.756	1.753
∠OCC	96.8	96.3	95.9
^{3}TCD−^{1}EPO[c]			
O−O	1.696	1.706	1.730
∠OCC	94.5	94.3	94.6

[a] Angstroms and degrees. [b] Plus singlet dioxygen. [c] Plus triplet dioxygen.

the breaking bond and the OCC angle which is closing upon the formation of the epoxide ring, Table 3 shows that little variations are found in going from one model to the other. The transition structure ^{1}TCD−^{1}EPO is shown in Figure 4b for M24.

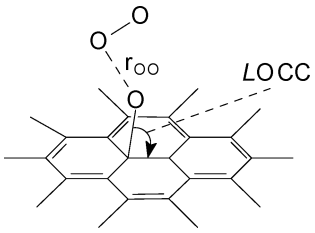

One point of interest is to assess the extent of competition between the pathway going through the primary ozonide and that involving the peroxyl diradical (energy profiles in Figure 5). If the rate of formation for EPO is defined as $v_{EPO} = v_{TCD} + v_{PO}$, disregarding pathways affected by an ISC, a steady-state treatment of the R−TCD−EPO vs R−PO−EPO pathways (Supporting Information) provides an estimate of the v_{TCD}/v_{PO} ratio of $10^{10}-10^{13}$. The only important way of functionalizing PAHs *on internal positions* seems to be described by the trioxyl diradical pathway.

3.5. Refinement of the Molecular Calculations. The energy barriers relevant to the preferred pathway were reassessed by a series of computations with a more extended basis set (Table 4).

3.6. Comparison with Experiments. In their careful experimental study on the reaction of O_3 with soot, KMNSS[8] considered several reactions involving soot and ozone. Following KMNSS, the very first step is the process

$$SS + O_3 \rightarrow SSO + O_2 \qquad (R1)$$

which is fast relative to other subsequent reactions (which will be further examined by us in our forthcoming work). In R1, SS is a surface site and SSO is the corresponding oxidized surface site. KMNSS measured the concentration of the oxidized surface site, by determining the O_2 production by mass spectroscopy, while knowing the surface area of the soot specimen. The measured surface concentration of SSO sites is $^1/_6$, with respect to the surface carbon atoms, assuming a graphitic model of soot for the surface. This large concentration of SSO sites indicates that all the graphitic surface is involved by the oxidation process.

Within our 2D periodic ab initio model, we could find a single energy minimum, an epoxidic $\sqrt{3}\times\sqrt{3}$ structure, described in Figure 6. The structure shown has C−O bond lengths of 1.457 Å, and the C−C bond of the triatomic ring is 1.350 Å (while the C−C distance in the graphite substrate is 1.423 Å). The C′ atoms belonging to the triatomic rings show a slight pyramidalization. It can be expressed by the angle of C′ with the two adjacent carbons, CC′C, which is 117° wide, so departing a little from the 120° value of graphite. Therefore, both the molecular and periodic models confirm that oxygen chemisorption corresponds to an epoxidic structure. In Table 5, the formation energies of the epoxidic structures (EPOs) are reported.

TABLE 4: 6-311G(2d) Energies[a] and Estimates of the Free Energies[a] for the Preferred Pathway

substrate[b] structure[c]		M16	M24	M42
R−^{1}TCD	E_1	21.1 (31.4)	19.8 (30.4)	13.7 (24.3)
	E	*19.2 (29.5)*	*17.9 (28.6)*	*11.4 (21.9)*
^{1}TCD anti	E_1	20.4 (30.2)	18.9 (29.1)	12.9 (23.1)
	E	*20.9 (30.7)*	*19.3 (29.5)*	*13.1 (23.3)*
^{1}TCD−EPO[d]	E_1	23.6 (23.6)	22.5 (31.6)	14.7 (24.3)

[a] Relative to the reactants; E_1, and E values, see footnote in Table 1. All values are in kcal mol^{-1}. The estimate of the free energies (in parentheses) are obtained by combining the 6-31G(d) data from the vibrational analysis with the 6-311G(2d) energies. [b] See Figure 1. [c] Labels, see Scheme 1. Transition structures are identified by the labels of the minima they connect. [d] From anti-TCD. [e] Plus $^3O_2$.

TABLE 5: Formation Energies[a] of the Epoxide Structures

substrate[b]	ΔE (EPO)[c]	ΔE (def)[d]
M10	−16.5	27.4
M16	−17.7[c]	27.2
M24	−15.0	27.7
M42	−23.9	21.9
P$\sqrt{3}\times\sqrt{3}$	−22.7	20.5
P3×3	−23.4	15.6

[a] kcal mol^{-1}. [b] See Figures 1 and 2. [c] Energy for epoxide formation. [d] Deformation energy of the substrate (see text).

The reaction energy for R1 provides an indication of the stability of the EPO structure for all the substrates. Though different epoxide isomers are possible for our M*n* models, only the most internal one has been considered in this paper, in which a surface adsorption process is investigated (naphthalene, the simplest PAH, cannot present a solely internal bond for ozone attack and is presented here only for comparative purposes).

The second column of Table 5 reports the deformation energies, calculated as the difference in substrate energies between the EPO geometry (without oxygen) and the free PAH geometry. These data suggest some importance of geometric and electronic factors in the PAH series upon functionalization. The smaller PAHs present, with respect to M42, a larger deformation energy and, in a parallel fashion, a smaller reaction energy. Though the originally planar sp^2 carbon atoms undergo pyramidalization upon epoxidation in all systems, the electronic perturbation of the aromatic situation is distributed on more extended molecular orbitals.

Finding an epoxide structure as the stable reaction product of ozone with undefective soot models, both molecular and periodic, is also coherent with the conclusions of the experimental study of the ozonization of fullerene.[37]

Finally, we have attempted to estimate the sticking coefficient or reaction probability γ. The sticking coefficient is defined in surface chemistry (see the IUPAC Compendium of Chemical Terminology, 2nd Ed., 1997) as the ratio of the rate of adsorption to the rate at which the adsorptive strikes the total surface, that is, covered and uncovered. As such, it is usually a function of surface coverage, of temperature, and of the details of the surface structure of the adsorbent. This coefficient was estimated in the experimental studies of FMBSO[7] and of KMNSS[8] as $\gamma_{exp} = 3.3 \times 10^{-3}$ (compare formula 1 in ref 8), relative to the initial

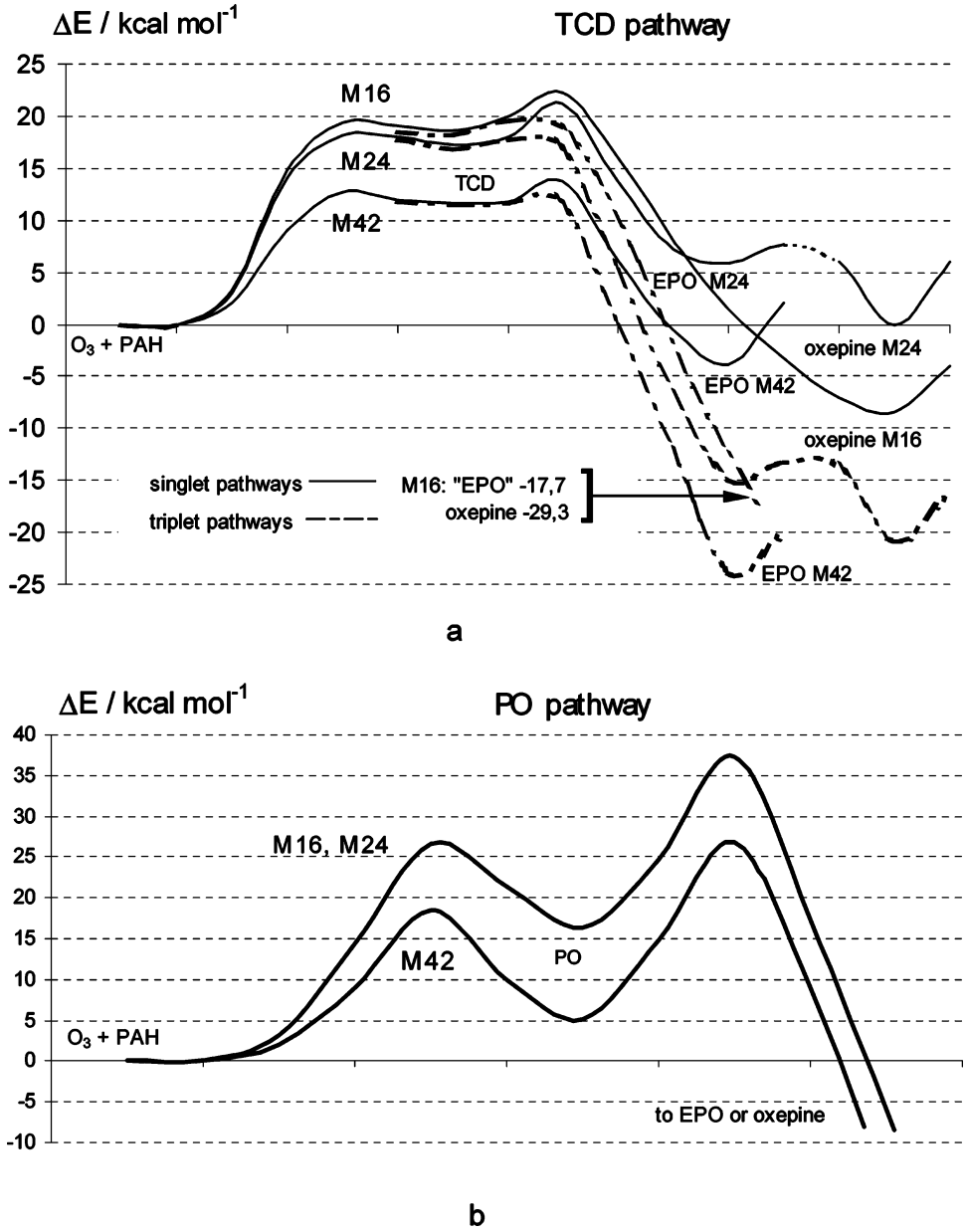

Figure 5. Energy profiles for the two reaction pathways defined (a) through the primary ozonides to the epoxides and (b) through the diradicals to the epoxides.

surface adsorption of ozone. Such a large value is interpreted as a fast process. The following analysis of the chemisorption process makes use of the kinetical analysis of the reaction, as described above. We estimate the sticking coefficient γ_{theor} by transition state theory (TST) following methods described by Pitt, Gilbert, and Ryan[38] and by Chorkendorff and Niemantsverdriet.[39] Thus, we adopt a Langmuir model, which is based on the following assumptions: (i) there are no interadsorbate interactions, (ii) the adsorbates are localized in equivalent sites on a homogeneous surface, (iii) the occupation of a site excludes further adsorption in that site, and (iv) only a monolayer adsorption is possible. If we hypothesize a Langmuir adsorption, considering a reaction barrier, for the rate-determining step (via R−TCD) of 12.9 kcal mol^{-1} (for the largest M42 substrate), we obtain a sticking coefficient γ_{theor} of the order of 10^{-13}. If we make the assumption of a Langmuir adsorption, using TST theory, then the sticking coefficient γ_{theor} can be calculated as $\gamma_{\text{theor}} = (k_B T/h) q^{\ddagger}/q_R \exp(-\Delta E^{\ddagger}/k_B T)/\nu$. In this formula, k_B is the Boltzmann constant, T the absolute temperature, and h is the Planck constant. $q^{\ddagger}/q_R$ is the ratio between the molecular partition functions of the transition state (critical dividing surface of the potential energy surface) and the molecular partition surface of the reactant. In the case of R−TCD transition state of the M42 model, $q^{\ddagger}/q_R = 6.7 \times 10^{-15}$. This value comes essentially from the product of the ratio between the vib-rotational partition functions of the O_3 molecule in the transition state and free in the gas phase (4.6×10^{-4}) times the ratio between the 2D and the 3D translational partition function of O_3, for unit volume and surface (1.5×10^{11}). Then, $\Delta E^{\ddagger}$ is the activation energy barrier with respect to the reactants corrected for the zero point energy. For the R−TCD transition structure in the case of the M42 model, $\Delta E^{\ddagger} = 13.1$ kcal mol^{-1}. Finally, ν is the mean velocity of the O_3 molecule perpendicular to the adsorbent surface. At room temperature, $\nu = 9.1 \times 10^{1}$ ms^{-1}. These values give $\gamma_{\text{theor}} = 1.2 \times 10^{-13}$, in evident contrast with the experiments. If, on the other hand, we hypothesize an initial van der Waals barrierless physisorption of ozone on the graphene surface (phys), we estimate $\gamma_{\text{theor}} = 4.1 \times 10^{-3}$. A van der Waals complex between the graphenic substrate and the ozone molecule has been well characterized for the M42

substrate (see the Supporting Information). The distance between the surface and O_3 is 3.6 Å (close to the interlayer distance in graphite). The binding energy of the O_3 is 2.8 kcal mol^{-1}, obtained by summing 0.3 kcal mol^{-1}, calculated at the DFT-(B3LYP)/6-31G(d) level, and corrected for the basis set superposition error by the counterpoise method, plus 2.5 kcal mol^{-1} of dispersion energy, obtained by molecular mechanics.[40] In the case of barrierless physisorption, the sticking coefficient γ can be calculated as $\gamma = (k_B T/h)(q_p/q_R)(1/\nu)$. Here, q_p/q_R is the ratio between the molecular partition functions of the physisorbed system and reactants; q_p/q_R is the product of q_{vrp}/q_{vr} the ratio between the vib-rotation partition function of the O_3 molecule in the physisorbed and gas phases, and its value is 4.1×10^{-3} (due to the hindrance in the rotation along two axes parallel to the surface), times the ratio between the 2D and the 3D translational partition function of O_3. These values set the sticking coefficient at $\gamma_{theor} = 4.1 \times 10^3$. Then, reaction R1 can be interpreted by the following mechanism

$$O_3\ (gas) \rightarrow O_3\ (phys)$$

$$\gamma_{theor} = 4.1 \times 10^{-3}, \quad \gamma_{exp} = 3.3 \times 10^{-3}$$

$$O_3\ (phys) \rightarrow TCD$$

$$TCD \rightarrow EPO + O_2$$

To conclude, the adsorption mechanism cannot be of Langmuir type, which gives a γ on the order of 10^{-13}.

Making reference to the work of KMNSS,[8] we can put forward, on the basis of computational results, a theoretical hypothesis on the preferred reaction pathway and on the adsorbed phase (as described by our Figure 6, compare Figure 6 of ref 8). However, our theoretical hypothesis on the adsorption mechanism (line I in Table 2 of ref 8) is that the initial step is a van der Waals barrierless adsorption. Finally, we can suggest that the stable species described and the chemiluminescence related to the generation of singlet dioxygen could be observed in a laboratory study.

4. Conclusions

This study deals with the oxidative functionalization that soot platelets or PAHs can undergo as a consequence of an electrophilic attack by ozone. The graphene elements are modeled by PAHs and periodic calculations. Both molecular and periodic simulations of the oxidation processes of these substrates involve only their *internal positions*, that is, they exclude the carbon atoms located along the perimeter of the platelet (object of a forthcoming paper).

Though some different possible pathways are considered, only the PO and the TCD are found as energy minima (intermediates). Actually, the intervention of the diradical as a real intermediate is questionable, due to its easy redissociation: rather, we can imagine that a "diradicaloid zone" of the energy hypersurface is probed by the reacting system. In both cases, upon exoergic dioxygen loss, an overall energy barrier is overcome (22, 21, and 14 kcal mol^{-1} high) for the three molecular models of increasing size. Thus, the process becomes easier upon extension of the unsaturated system. Through this last step an EPO is formed. If the rate of formation for an EPO is defined as $\upsilon_{EPO} = \upsilon_{TCD} + \upsilon_{PO}$, a steady-state treatment of the R−TCD−EPO vs the R−PO−EPO pathways gives an estimate for the $\upsilon_{TCD}/\upsilon_{PO}$ ratio of $10^{10}-10^{13}$. It is then concluded that ozonization of internal positions has to pass through a region of the energy hypersurface where the system has diradical character.

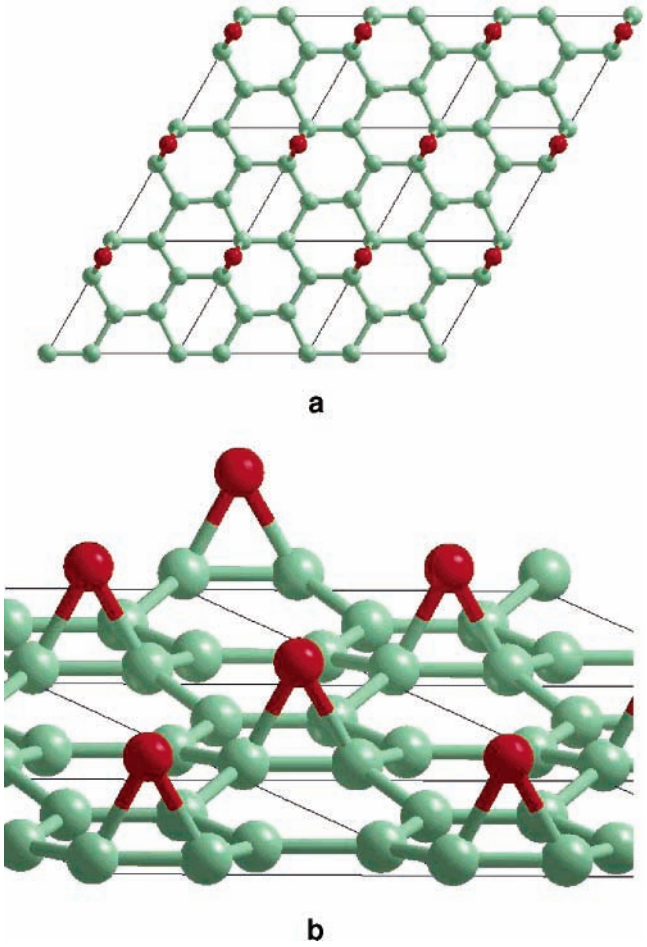

Figure 6. 2D periodic ab initio model of the graphenic plate with oxygen atoms chemisorbed to give an epoxidic functionalization: (a) top view, (b) side view.

If an atmospheric process is considered, then the barriers for the first attack appear to be too high to allow the ozonization of internal positions in a significant way, at least for the smallest PAHs and soot platelets. On the other hand, in an experiment employing large ozone concentrations, we can surmise that it can take place, but border ozonization should precede the massive ozonization of the internal positions. This point will be addressed in a follow-up paper.

If the spin multiplicity is conserved, either a $^1\Delta_g$ oxygen molecule moves off the singlet functionalized substrate or, as an alternative, ground-state dioxygen and a π-triplet epoxide might form. However, an ISC possibly occurs in correspondence of the trioxyl diradical intermediate, as suggested by the fact that the triplet and singlet states of this intermediate have very similar energies, geometries, and vibrational frequencies. If this were the case, ISC would give way to the production of both ground-state dioxygen and epoxide.

Acknowledgment. Financial support by the Italian MIUR is gratefully acknowledged (PRIN-COFIN 2003, "Studio di specie reattive cariche e neutre e di reazioni ione-molecola in fase gassosa", Cod. 2003035479). A.G. (Ph.D. student, Dottorato di Ricerca in Scienze Chimiche, XX ciclo) is supported by a generous grant provided by the Regione Piemonte. For the graphics, we exploited the MOLDEN program[41] and the

XCRYSDEN program.[42] The van der Waals energies were computed by the program MOLDRAW.[43]

Supporting Information Available: The geometries of all optimized structures, the corresponding total energies, and some information about atomic spin densities for structures with some diradicaloid traits are presented. This material is available free of charge via the Internet at http://pubs.acs.org.

References and Notes

(1) (a) Cooke, W. F.; Wilson, J. J. N. *J. Geophys. Res.* **1996**, *101*, 19395−19409. Liousse, C.; Penner, J. E.; Chuang, C.; Walton, J. J.; Eddleman, H.; Cachier, H. *J. Geophys. Res.* **1996**, *101*, 19411−19432. (b) Finlayson-Pitts, B. J.; Pitts, J. N., Jr. *Chemistry of the Upper and Lower Atmosphere*; Academic Press: San Diego, CA, 2000; Chapter 10, sections E and F. (c) Finlayson-Pitts, B. J.; Pitts, J. N., Jr. *Chemistry of the Upper and Lower Atmosphere*; Academic Press: San Diego, CA, 2000; Chapter 10, section A, § 4. (d) Finlayson-Pitts, B. J.; Pitts, J. N., Jr. *Chemistry of the Upper and Lower Atmosphere*; Academic Press: San Diego, CA, 2000; Chapter 10, sections B, C, and D.

(2) Homann, K.-H. *Angew. Chem., Int. Ed. Engl.* **1998**, *37*, 2435−2451.

(3) Kirchner, U.; Scheer, V.; Vogt, R. *J. Phys. Chem. A* **2000**, *104*, 8908−8915.

(4) Arens, F.; Gutzwiller, L.; Baltensperger, U.; Gäggeler, H. W.; Amman, M. *Environ. Sci. Technol.* **2001**, *35*, 2191−2199.

(5) Lu're, B. A.; Mikhno A. V. *Kinet. Catal.* **1997**, *38*, 490−497.

(6) Pöschl, U.; Letzel, T.; Schauer, C.; Niessner, R. *J. Phys. Chem. A* **2001**, *105*, 4029−4041. Schauer, C.; Niessner, R.; Pöschl, U. *Poster CMD-44 at the Eurotrac-2 2002 Symposium*; Garmish-Partenkierken, 2002.

(7) Fendel, W.; Matter, D.; Burtscher, H.; Schmidt-Ott, A. *Atmos. Environ.* **1995**, *29*, 967−973.

(8) Kamm, S.; Mohler, O.; Naumann K.-H.; Saathoff, H.; Schurath, U. *Atmos. Environ.* **1999**, *33*, 4651−4661.

(9) Kamens, R. M.; Guo, J.; Guo, Z.; McDow, S. R. *Atmos. Environ.* **1990**, *24A*, 1161−1173.

(10) Atkinson, R.; Arey, J. *Environ. Health Perspect.* **1994**, *102*, Suppl. 4, 117−126.

(11) Pitts, J. N., Jr.; Lokensgard, D. M.; Ripley, P. S.; van Cauwenberghe, K. A.; van Vaeck, L.; Schaffer, S. D.; Thill, A. J.; Belser, W. L. *Science* **1980**, *210*, 1347−1349.

(12) (a) Petzold, A.; Stein, C.; Nyeki, S.; Gysel, M.; Weingartner, E.; Baltensperger, U.; Giebl, H.; Hitzenberger, R.; Dopelheuer, A.; Vrchoticky, S.; Puxbaum, H.; Johnson, M.; Hurley, C. D.; Marsh, R.; Wilson, C. W.; *Geophys. Res. Lett.* **2002**, *30*, 1719−1722. Grothe, H.; Muckenhuber, H. *The Third Informal Conference on Reaction Kinetics and Atmospheric Chemistry*, Helsingør, Denmark, 2002. (b) Blake, D. F.; Kato, K. *J. Geophys. Res.* **1995**, *100*, 7195−7202. Peuschl, R. F.; Boering, K. A.; Verma, S.; Howard, S. D.; Ferry, G. V.; Goodman, J.; Allen, D. A.; Hamill, P. *J. Geophys. Res.* **1997**, *102*, 13113−13118.

(13) Ghigo, G.; Maranzana, A.; Tonachini, G.; Zicovich-Wilson, C. M.; Causà, M. *J. Phys. Chem. B* **2004**, *108*, 3215−3223.

(14) Ghigo, G.; Tonachini, G. *J. Am. Chem. Soc.* **1998**, *120*, 6753−6757. Ghigo, G.; Tonachini, G. *J. Am. Chem. Soc.* **1999**, *121*, 8366−8372. Ghigo, G.; Tonachini, G. *J. Chem. Phys.* **1999**, *109*, 7298−7304. Motta, F.; Ghigo, G.; Tonachini, G. *J. Phys. Chem. A* **2002**, *106*, 4411−4422.

(15) Lee, K. H.; Causà, M.; Park, S. S. *J. Phys. Chem. A* **1998**, *102*, 6020−6024.

(16) Chen, N.; Yang, R. T. *Carbon* **1998**, *36*, 1061−1070. Kiotani, T.; Tomita, A. *J. Phys. Chem. B* **1999**, *103*, 3434−3441.

(17) Montoya, A.; Mondragòn, F.; Truong, T. N. *Carbon* **2003**, *41*, 29−39 and references therein. Espinal, J. F.; Montoya, A.; Mondragòn, F.; Truong, T. N. *J. Phys. Chem. B* **2004**, *108*, 5405−5409. Hamad, S.; Mejias, J. A.; Lago, S.; Picaud, S.; Hoang, P. N. M. *J. Phys. Chem. B* **2004**, *108*, 5405−5409.

(18) (a) Pople, J. A.; Gill, P. M. W.; Johnson, B. G. *Chem. Phys. Lett.* **1992**, *199*, 557−560. Schlegel, H. B. In *Computational Theoretical Organic Chemistry*; Csizsmadia, I. G., Daudel, Eds.; Reidel Publ. Co.: Boston, MA, 1981; pp 129−159. Schlegel, H. B. *J. Chem. Phys.* **1982**, *77*, 3676−3681. Schlegel, H. B.; Binkley, J. S.; Pople, J. A. *J. Chem. Phys.* **1984**, *80*, 1976−1981. Schlegel, H. B. *J. Comput. Chem.* **1982**, *3*, 214−218. (b) Gonzalez, C.; Schlegel, H. B. *J. Chem. Phys.* **1989**, *90*, 2154−2161. Gonzalez, C.; Schlegel, H. B. *J. Phys. Chem.* **1990**, *94*, 5523−5527 and references therein.

(19) Parr, R. G.; Yang, W. *Density Functional Theory of Atoms and Molecules*; Oxford University Press: New York, 1989; Chapter 3. Becke, A. D. *Phys. Rev. A* **1988**, *38*, 3098−3100. Becke, A. D. *ACS Symp. Ser.* **1989**, *394*, 165. Pople, J. A.; Gill, P. M. W.; Johnson, B. G. *Chem. Phys. Lett.* **1992**, *199*, 557−560. Becke, A. D. *J. Chem. Phys.* **1993**, *98*, 5648−5652. Lee, C.; Yang, W.; Parr, R. G. *Phys. Rev. B* **1988**, *37*, 785−789.

(20) Jensen, F. *Introduction to Computational Chemistry*; John Wiley & Sons: New York, 1999; Chapter 6.

(21) 6-31G: Hehre, W. J.; Ditchfield, R.; Pople, J. A. *J. Chem. Phys.* **1972**, *56*, 2257−2261. 6-31G(d): Hariharan, P. C.; Pople, J. A. *Theor. Chim. Acta* **1973**, *28*, 213−222. Multiple polarization functions: Frisch, M. J.; Pople, J. A.; Binkley, J. S. *J. Chem. Phys.* **1984**, *80*, 3265−3269.

(22) Gordon, M. S.; Binkley, J. S.; Pople, J. A.; Pietro, W. J.; Hehre, W. J. *J. Am. Chem. Soc.* **1982**, *104*, 2797. Pietro, W. J.; Francl, M. M.; Hehre, W. J.; Defrees, D. J.; Pople, J. A.; Binkley, J. S. *J. Am. Chem. Soc.* **1982**, *104*, 5039. A value of 0.240 was employed instead of the standard 0.187. In periodic LCAO calculations, the basis set needs to be slightly modified, regarding the more expanded functions, to avoid the numerical consequences of a badly defined exchange potential or the quasi-linear dependency of the basis function (see ref 28c). This is even more important for conductive materials such as graphite. The exponential coefficients of the three sp Gaussian functions used as the internal valence linear combination in the 6-31G carbon basis set are 7.87, 1.88, and 0.54. If the value of the external valence coefficient is increased from 0.197 to 0.24, as requested by periodic LCAO calculations, numerical linear dependence problems are avoided. On the other hand, this problem is absent with the 6-21G basis set, where the exponential coefficients of the two internal valence Gaussians are 3.66 and 0.77.

(23) Maranzana, A.; Ghigo, G.; Tonachini, G. *J. Am. Chem. Soc.* **2000**, *122*, 1414−1423. Maranzana, A.; Ghigo, G.; Tonachini, G. *Chem.−Eur. J.* **2003**, *9*, 2616−2626.

(24) Seeger, R.; Pople, J. A. *J. Chem. Phys.* **1977**, *66*, 3045−3050. Bauernschmitt, R.; Ahlrichs, R. *J. Chem. Phys.* **1996**, *104*, 9047−9052. Schlegel, H. B.; McDouall, J. J. In *Computational Advances in Organic Chemistry*; Ogretir, C., Csizmadia, I. G., Eds.; Kluwer Academic: The Netherlands, 1991; p 167.

(25) Yamanaka, S.; Kawakami, T.; Nagao, K.; Yamaguchi, K. *Chem. Phys. Lett.* **1994**, *231*, 25−33. Yamaguchi, K.; Jensen, F.; Dorigo, A.; Houk, K. N. *Chem. Phys. Lett.* **1988**, *149*, 537−542. Cramer, C. J.; Dulles, F. J.; Giesen, G. J.; Almlöf, J. *Chem. Phys. Lett.* **1995**, *245*, 165−170. Goldstein, E.; Beno, B.; Houk, K. N. *J. Am. Chem. Soc.* **1995**, *118*, 6036−6043

(26) Reaction enthalpies and entropies were computed as outlined, for instance, in Foresman, J. B.; Frisch, *Æ. Exploring Chemistry with Electronic Structure Methods*; Gaussian, Inc.: Pittsburgh, PA, 1996; pp 166−168. McQuarrie, D. A. *Statistical Thermodynamics*; Harper and Row: New York, 1973; Chapter 8. How the thermochemical quantities are dealt with in GAUSSIAN03 is documented in http://www.Gaussian.com/g_whitepap/thermo.htm. In our study, the vibrational frequencies were not scaled, which is the default procedure in GAUSSIAN03. However, a test was carried out on the diradical reaction path of coronene, by scaling the frequencies by the factor 0.9806, suggested in Scott, A. P.; Radom, L. *J. Phys. Chem.* **1996**, *100*, 16502−16513. The maximum (positive) variation in free energy barriers introduced by scaling was 0.4 kcal mol^{-1}.

(27) Frisch, M. J.; Trucks, G. W.; Schlegel, H. B.; Scuseria, G. E.; Robb, M. A.; Cheeseman, J. R.; Zakrzewski, V. G.; Montgomery, J. A., Jr.; Stratmann, R. E.; Burant, J. C.; Dapprich, S.; Millam, J. M.; Daniels, A. D.; Kudin, K. N.; Strain, M. C.; Farkas, O.; Tomasi, J.; Barone, V.; Cossi, M.; Cammi, R.; Mennucci, B.; Pomelli, C.; Adamo, C.; Clifford, S.; Ochterski, J.; Petersson, G. A.; Ayala, P. Y.; Cui, Q.; Morokuma, K.; Malick, D. K.; Rabuck, A. D.; Raghavachari K.; Foresman, J. B.; Cioslowski, J.; Ortiz, J. V.; Stefanov, B. B.; Liu, G.; Liashenko, A.; Piskorz, P.; Komaromi, I.; Gomperts, R.; Martin, R. L.; Fox, D. J.; Keith, T.; Al-Laham, M. A.; Peng, C. Y.; Nanayakkara, A.; Gonzalez, C.; Challacombe, M.; Gill, P. M. W.; Johnson, B.; Chen, W.; Wong, M. W.; Andres, J. L.; Head-Gordon, M.; Replogle, E. S.; Pople, J. A. *Gaussian 98*; Gaussian, Inc.: Pittsburgh, PA, 1998.

(28) (a) Saunders, V. R.; Dovesi, R.; Roetti, C.; Orlando, R.; Zicovich-Wilson, C. M.; Harrison, N. M.; Doll, K.; Civalleri, B.; Bush, I. J.; D'Arco, Ph.; Llunell, M. *CRYSTAL 2003 User Manual*; Turin University: Turin, Italy, 2003. (b) Saunders, V. R.; Dovesi, R.; Roetti, C.; Causà, M.; Harrison, N. M.; Zicovich-Wilson, C. M. *CRYSTAL'98 User Manual*; Turin University: Turin, Italy, 1999. (c) Pisani, C.; Dovesi, R.; Roetti, C. *Hartree−Fock Ab Initio Treatment of Crystalline Systems, Lecture Notes in Chemistry*; Springer-Verlag: Heidelberg, Germany, 1988; Vol. 48.

(29) Dovesi, R.; Pisani, C.; Roetti, C.; Saunders, V. R. *Phys. Rev. B* **1983**, *28*, 5781−5792.

(30) Causà, M.; Dovesi, R.; Orlando, R.; Pisani, C.; Saunders, V. R. *J. Phys. Chem.* **1988**, *92*, 909−913.

(31) Pisani, C.; Aprà, E.; Causà, M. *Int. J. Quantum Chem.* **1990**, *38*, 395−417.

(32) Zicovich-Wilson, C. M.; Dovesi, R. *Int. J. Quantum Chem* **1998**, *67*, 299−309.

(33) Doll, K.; Harrison, N. M.; Saunders, V. R. *Int. J. Quantum Chem.* **2001**, *82*, 1−12. Doll, K. *Comput. Phys. Commun.* **2001**, *137*, 74−82. Civalleri, B.; D'Arco, Ph.; Orlando, R.; Saunders, V. R.; Dovesi, R. *Chem. Phys. Lett.* **2001**, *348*, 131−138.

(34) As the graphite layers are weakly bound by van der Waals forces, which density functional models cannot described correctly (ref 39), we ascertained in our first paper (ref 13) the adequacy of a model constituted

by a single layer. In fact, a second graphene layer affected insignificantly the surface chemical properties and only weakly the surface density (ref 35). The hydrogen adsorption energy, in the presence of one or two layers, gave the very close adsorption energies within the P3×3 model: −18.7 and −17.3 kcal mol^{-1}, respectively.

(35) Kristyan, S.; Pulay, P. *Chem. Phys. Lett.* **1994**, *229*, 175−180. Perez-Jorda, J. M.; Becke, A. D. *Chem. Phys. Lett.* **1995**, *233*, 134−137. Meijer, E. J.; Sprik, M. *J. Chem. Phys.* **1996**, *105*, 8684−8689. Tsuzuki, S.; Lûthi, H. P. *J. Chem. Phys.* **2001**, *114*, 3949−3957. See also, for a DFT approach not based on the Kohn−Sham equations: Tran, F.; Weber, J.; Wesołowski, T. A. *Helv. Chim. Acta* **2001**, *84*, 1489−1503. For the use of Møller−Plesset methods to model the interlayer interactions in graphite: Ruuska, H.; Pakkanen, T. A. *J. Phys. Chem. B* **2001**, *105*, 9541−9547.

(36) Borrelli, R.; Causà, M.; Maranzana, A.; Peluso, A.; Tonachini, G. To be submitted for publication. Results presented at the 34th Congress of the Physical Chemistry Division of the Italian Chemical Society, Siena, Italy, June, 2005.

(37) Heymann, D.; Bachilo, S. M.; Weisman, R. B.; Cataldo, F.; Fokkens, R. H.; Nibbering, N. M. M.; Vis, R. D.; Chibante, L. P. F. *J. Am. Chem. Soc.* **2000**, *122*, 11473−11479.

(38) Pitt, I. G.; Gilbert, R. G.; Ryan, K. R. *J. Chem. Phys.* **1995**, *102*, 3461−3473.

(39) Chorkendorff, I.; Niemantsverdriet. J. W. *Concepts of Modern Catalysis and Kinetics*; Wiley-VCH Verlag: Weinheim, Germany, 2003.

(40) Spackman, M. A. *J. Chem. Phys*. **1986**, *85*, 11.

(41) MOLDEN: Schaftenaar, G.; Noordik, J. H. *J. Comput.-Aided Mol. Design*, **2000**, *14*, 123−134. http://www.cmbi.ru.nl/molden/molden.html.

(42) XCRYSDEN: Kokalj, A. *Comput. Mater. Sci.* **2003**, *28*, 155. Code available from http://www.xcrysden.org/.

(43) Ugliengo, P.; Viterbo, D.; Chiari, G. *Z. Kristallogr*. **1993**, *207*, 9. http://www.moldraw.unito.it/.